



Improved performance-based seismic coefficient for gravity-type quay walls based on centrifuge test results

Moon-Gyo Lee¹ · Jeong-Gon Ha² · Hyung-Ik Cho¹ · Chang-Guk Sun¹ · Dong-Soo Kim³

Received: 9 April 2020 / Accepted: 22 September 2020 / Published online: 6 October 2020
© Springer-Verlag GmbH Germany, part of Springer Nature 2020

Abstract

Verifying the seismic performance of port structures when the force balance limit is exceeded is important for the performance-based seismic design of gravity-type quay walls. Over the last three decades, performance verification methods have been developed that consider the effects of the design earthquake motion, geotechnical conditions, and structural details on the deformation of a quay wall to accurately predict earthquake-induced damage. In this study, representative performance verification methods (i.e., simplified dynamic analysis methods extending from the Newmark sliding block method and performance-based seismic coefficients developed in Japan) were quantitatively assessed with actual cases of earthquake-damaged quay walls and the results of dynamic centrifuge tests previously conducted under various conditions (i.e., different wall heights, earthquake motions and the thickness of subsoil). The dynamic centrifuge test results suggested directions for improving the performance-based seismic coefficients of the representative methods, while their field applicability and reliability were confirmed according to the actual earthquake records.

Keywords Dynamic centrifuge test · Gravity-type quay wall · Newmark sliding block theory · Seismic code · Seismic coefficient · Time–frequency analysis

1 Introduction

Quay walls are a typical mooring facility. Conventionally, their seismic performance is evaluated through simplified analysis based on the pseudo-static method, simplified dynamic analysis based on the sliding block method, or dynamic analysis using finite element or finite difference numerical techniques [2, 9, 12, 14, 22, 23, 37, 38, 40]. Since the Great Hanshin Earthquake-damaged Kobe Port in 1995, significant advances have been made in dynamic analysis, which can comprehensively consider soil–structure interaction and soil nonlinear behavior in response to

an earthquake, and performance-based design has been introduced for port structures. However, challenges remain for dynamic analysis in that the results differ depending on the designer’s understanding of the numerical analysis and the selection of input parameters such as those for the constitutive models, mesh discretization, and material properties. Therefore, simplified analysis and simplified dynamic analysis, which offer the advantages of being capable of quickly and easily evaluating the seismic stability of structures, are still widely used in countries that apply prescriptive seismic design based on national seismic codes for the sake of practicality [9, 14, 22, 23, 40, 49].

In the simplified analysis, the active thrust is calculated by adopting the Coulomb earth pressure theory to determine the magnitude of the soil thrust acting on the wall and the Mononobe–Okabe (M–O) [42, 50] method to consider the seismic earth pressure. For the M–O method, defining an appropriate seismic coefficient (k_h) is crucial for obtaining an analysis result close to the real seismic response because the earthquake motion is transduced to an equivalent pseudo-static inertial force through k_h .

✉ Dong-Soo Kim
dskim@kaist.ac.kr

¹ Earthquake Research Center, Korea Institute of Geoscience and Mineral Resources, Daejeon, Korea

² Structural Safety and Prognosis Research Division, Korea Atomic Energy Research Institute, Daejeon, Korea

³ Department of Civil and Environmental Engineering, Korea Advanced Institute of Science and Technology, Daejeon, Korea

The conventional k_h is simply defined as the peak ground acceleration (PGA) of the design ground motion, which is determined through a probabilistic seismic hazard analysis, divided by the acceleration of gravity (g). It does not sufficiently reflect the characteristics of real dynamic motions and is conservative. To improve the definition of k_h to consider the seismic performance of a quay wall and site amplification effects, several methods have been considered, such as applying a correction factor according to the allowable deformation of the quay wall crown (D_a) [14, 23, 37, 40, 60] or changing the selected PGA location for calculating k_h according to the wall height (H_w) [14, 22, 23, 33, 40]. The representative definitions of k_h are summarized in Table 1.

However, the simplified analysis does not provide information on the performance of a structure when the force balance limit is exceeded. Various studies have focused on the effects of the frequency characteristics of the input earthquake [10, 17, 18, 44, 49], stiffness of the soil [20, 21, 43], and phase characteristics of the wall inertial forces and dynamic earth pressure [1, 8, 10, 45, 54, 57, 58] on the deformation of the quay wall (D_h) to overcome this limitation.

The simplified dynamic analysis adopts the Newmark sliding block theory [47] to evaluate D_h during earthquakes. This theory obtains D_h by double integration of the given design earthquake acceleration time history with the critical acceleration (a_{cr}) used as the reference datum. Here, a_{cr} is defined as the minimum horizontal acceleration resulting in a safety factor of 1 for sliding failure of the

wall–backfill system. Because the M–O method is used to evaluate the sliding stability of the wall and backfill, simplified dynamic analysis adopts similar assumptions as simplified analysis.

Most simplified dynamic analysis methods are extensions of the Newmark theory to improve a certain functional relationship between the expected D_h , a_{cr} , and representative characteristic parameters of the earthquake record (MP). Representative simplified dynamic analysis methods are listed in Table 2. The main assumptions and limitations of each method are well described by Al-Homoud and Tahtamoni [2], Cai and Bathurst [9], Deyanova et al. [12], and Meehan and Vahedifard [36]. Simplified dynamic analysis methods do not include variables related to soil conditions or the geometric characteristics of the wall. MP consists of the PGA and peak ground velocity (PGV) and does not fully reflect the frequency components below 1 Hz, which are known to be primarily related to D_h induction, or the duration. Because the proposed simplified dynamic analysis methods cannot accurately predict D_h owing to earthquakes, various studies have focused on determining MP to consider the characteristics closely related to D_h induction [8, 12, 13, 16, 28, 30, 36, 44].

To consider the research trends described above, the Ministry of Land, Infrastructure and Transport (MLIT) [38] in Japan proposed the concept of a performance-based seismic coefficient (k_{hk}) to verify the performance of port structures exceeding the force balance limit in place of k_h in the M–O method. This concept was derived from the work of Nagao and Iwata [44], who used the finite element

Table 1 Overview of the representative seismic coefficient (k_h) definitions (modified from Lee et al. [33])

| Codes/Guidelines | Equations | Correction factor (r) | | Reference PGA (a_{max}) | |
|------------------|--|-----------------------|---|-----------------------------|------------------|
| | | | | H_w over 10 m | H_w under 10 m |
| EN [14] | $k_h = \frac{1}{r} \frac{a_{max}}{g}$ | 2 | Free gravity walls that can accept a displacement up to $D_a = 300 \cdot a_{max}$ (mm) | Average PGA**** | Base PGA** |
| | | 1.5 | Free gravity walls that can accept a displacement up to $D_a = 200 \cdot a_{max}$ (mm) | | |
| | | 1 | Flexural reinforced concrete walls, anchored or braced walls, reinforced concrete walls founded on vertical piles | | |
| MOF [40] | $k_h = \frac{1}{r} \frac{a_{max}}{g}$ | 2 | $D_a = 300$ (mm) | Surface PGA*** | Base PGA** |
| | | 1 | $D_a = 0$ (mm) | | |
| MLIT [37] | $k_h = \frac{1}{r} \left(\frac{a_{max}}{g} \right)^{\frac{1}{r}}$ | 1 | $a_{max} < 0.2$ | Special class* | Surface PGA*** |
| Werner [60] | | 3 | $a_{max} > 0.2$ | | |
| | $k_h = r \frac{a_{max}}{g}$ | 0.6 | Class B* | | |
| MOLIT [39] | $k_h = \frac{a_{max}}{g}$ | N/A | N/A | Average PGA**** | |

*Detailed in MLIT [37]

**PGA of the design ground motion determined through a probabilistic seismic hazard analysis

***PGA of the acceleration motion on the backfill surface obtained from a 1D site response analysis using the design ground motion

****Average PGA of the acceleration motions along the wall height obtained from a 1D site response analysis using the design ground motion

Table 2 Overview of the representative simplified dynamic analysis methods

| References | Equation | Remark |
|-----------------------|--|------------------|
| Newmark [47] | $D_h = \frac{(PGV)^2}{2a_{cr}} \left(1 - \frac{a_{cr}}{PGA}\right) \left(\frac{a_{cr}}{PGA}\right)^{-2}$ | Upper bound |
| Ambraseys [3] | $D_h = 10 \frac{(2.3-3.3 \frac{a_{cr}}{PGA})}{100}$ | Upper bound |
| Richard and Elms [53] | $D_h = \frac{0.087PGV^2PGA^3}{a_{cr}^2}$ | Upper bound |
| Cai and Bathurst [9] | $D_h = \frac{35PGV^2}{PGA} \exp\left(\frac{-6.91a_{cr}}{PGA}\right) \left(\frac{a_{cr}}{PGA}\right)^{-0.38}$ | Mean upper bound |
| Whitman and Liao [61] | $D_h = \frac{37PGV^2}{PGA} \exp\left(\frac{-9.4a_{cr}}{PGA}\right)$ | Mean fit |
| Zarrabi [62] | $D_h = R_v R_z \frac{37PGV^2}{PGA} \exp\left(\frac{-9.4a_{cr}}{PGA}\right)$ | Mean fit |
| | $R_v = 1.015 - 0.2 \frac{a_{cr}}{PGA} + 0.72 \left(\frac{a_{cr}}{PGA}\right)^2$ | |
| | $R_z = 0.7 + 1.2 \frac{a_{cr}}{PGA} \left(1 - \frac{a_{cr}}{PGA}\right)$ | |

analysis program (FLIP) to perform two-dimensional total stress analysis on quay wall models under various conditions for a_{cr} , H_w , frequency of the input motion, and stiffness of the soil. They numerically modeled all combinations of the above conditions and derived the PGA values for all the cases when D_h reached 20 cm by adjusting the intensities of sinewaves for various frequencies (i.e., 0.2, 0.3, 0.4, 0.6, 0.8, 1.0, 1.5, 2.0, 3.0, and 4.0 Hz). Through the derived results, they proposed the following b filter to make the filtered peak acceleration (a_f) converge to the target a_{cr} regardless of H_w , the frequency of the input motion (f), the initial natural period of the backfill ground (T_b), and the initial natural period of the subsoil underneath the wall (T_u). The b filter equation, which is flat below 1 Hz and rapidly attenuates at frequencies exceeding 1 Hz, has been derived using the regression analysis of b with three independent variables— H_w , T_u , and T_b —affecting the frequency characteristics of ground motion.

$$a(f) = b, 0 < f \leq 1.0 \tag{1a}$$

$$a(f) = \frac{b}{1 - \left(\frac{f-1.0}{1/0.34}\right)^2 + 6.8 \left(\frac{f-1.0}{1/0.34}\right) i}, 1.0 < f \tag{1b}$$

$$b = 1.05 \frac{H_w}{H_{wR}} - 0.88 \frac{T_b}{T_{bR}} + 0.96 \frac{T_u}{T_{uR}} - 0.23 \tag{1c}$$

$$0.04H_w + 0.08 \leq b \leq 0.04H_w + 0.44 \tag{1d}$$

where a is the b filter, considering the frequency characteristics of the input earthquake, f is the frequency (Hz), H_w is the wall height (m), H_{wR} is the standard wall height (15 m), T_b is the initial natural period of the backfill ground

(s), T_{bR} is the standard initial natural period of the backfill ground (0.8 s), T_u is the initial natural period of the subsoil underneath the wall (s), T_{uR} is the standard initial natural period of the subsoil underneath the wall (0.4 s), and i is an imaginary unit. b should be set in a range determined by Eq. 1d with H_w . Regardless of the range in Eq. 1d, the lower limit should not be less than 0.28 in all cases.

Nagao and Iwata [44] used nine measured earthquake records to verify that the a_f values, which make the D_h of the quay walls with various target a_{cr} values to 20 cm, converged to the target a_{cr} values. Their analysis results indicated various differences between a_f and the target a_{cr} for each earthquake record. This difference was assumed to be due to the various durations of each earthquake record. By regression analysis, they derived the following reduction factor (P) that can be multiplied with a_f to obtain the duration-corrected peak acceleration (a_c):

$$P = 0.36 \ln(S/a_f) - 0.29 \tag{2}$$

where P is the reduction factor ($P \leq 1.0$), S is the root sum square of the acceleration time history after filtering (cm/s^2), and a_f is the maximum acceleration obtained after filtering (cm/s^2).

Finally, Nagao and Iwata [44] used the nine measured earthquake records to find all a_c values that result in the other D_a values (i.e., 5, 10, and 15 cm) for quay walls designed with various target a_{cr} values. Then, they performed a regression analysis with both the obtained a_c values and the set values of D_a to derive k_{hk} , which is the seismic coefficient corresponding to D_a :

$$k_{hk} = 1.78 \left(\frac{D_a}{D_r} \right)^{-0.55} \frac{a_c}{g} + 0.04 \quad (3)$$

where k_{hk} is the characteristic value of the seismic coefficient for verification, a_c is the maximum corrected acceleration (cm/s^2), g is the gravitational acceleration (980 cm/s^2), D_a is the allowable deformation of the quay wall, and D_r is the standard deformation of the quay wall (10 cm).

The procedure for calculating k_{hk} was detailed by the MLIT [38] and is briefly summarized below:

- (1) The acceleration time history on the ground surface is calculated by performing an one-dimensional site response analysis using a level 1 earthquake ground motion determined through a probabilistic seismic hazard analysis as the input.
- (2) A fast Fourier transform (FFT) is performed on the surface acceleration time history to obtain the acceleration spectrum of the ground surface.
- (3) The filtered acceleration spectrum is obtained by filtering the surface acceleration spectrum with a b filter (Eq. 1a).
- (4) a_f is obtained from the acceleration time history following an inverse FFT operation on the filtered spectrum.
- (5) a_c at the ground surface is obtained by multiplying a_f by P (Eq. 2).
- (6) Finally, k_{hk} is obtained by substituting a_c and D_a into Eq. 3. This method is applicable when $D_a = 5\text{--}20 \text{ cm}$.

The k_{hk} concept was validated by Fukunaga et al. [15] and Lee et al. [32], who used real case histories of gravity-type quay walls during earthquakes and dynamic centrifuge test results, respectively. Their results indicated that k_{hk} can be used to accurately predict the performance of port structures exceeding the force balance limit in general. However, they also confirmed the need for improvement because this approach evaluates D_h relatively conservatively for cases where low-frequency components are dominant.

This study analyzed incidents of earthquake-induced damage to quay walls in Japan and Korea and the dynamic centrifuge test results presented by Lee et al. [32] to quantitatively evaluate the performance of the representative simplified dynamic analysis methods and the k_{hk} concept. In addition, the dynamic centrifuge test results were used to improve the b filter included in the k_{hk} concept, and the improvements were verified according to actual cases of earthquake-damaged quay walls.

2 Methodology

2.1 Assessment of simplified dynamic analysis methods and the k_{hk} concept using actual cases of earthquake-damaged quay walls

Over the last three decades, various methods (i.e., the simplified dynamic analysis methods summarized in Table 2 and the k_{hk} concept) have been proposed to improve the prediction accuracy for the performance of quay walls subjected to design earthquake motions. However, few efforts have been made to quantitatively evaluate the accuracy of these proposed methods by comparing them with actual measurements of D_h for quay walls damaged by earthquakes [2, 7, 9, 36]. Therefore, this study evaluated the prediction accuracy for D_h of the proposed methods by comparing the actual D_h values from real cases of gravity-type quay walls damaged by earthquakes with those obtained by inputting the real field conditions into the proposed methods.

Fukunaga et al. [15] recently summarized information on damage to quay walls caused by earthquakes that occurred throughout Japan: the structural details, geotechnical conditions, and acceleration time histories caused by earthquakes. Their data were provided by the National Institute for Land and Infrastructure Management (NILIM) and Port and Airport Research Institute (PARI). In the present study, this information was used for a quantitative analysis of the proposed methods. Cases that met the following conditions were selected for analysis: gravity-type walls, mainly sliding failure occurred, and D_h was within 30 cm. Furthermore, a moment magnitude (M) 5.4 earthquake occurred in Pohang City in the southeastern part of the Korean peninsula on 15 November 2017, and lateral spreading took place at a gravity-type quay wall in Youngil Bay Port approximately 6 km away from the main shock epicenter [25]. The Ministry of Oceans and Fisheries (MOF) investigated the damage to the quay wall in detail, and the reported data were also used in this study [41].

The information and backfill surface ground motion on the eight cases selected for the quantitative evaluation are summarized in Table 3 and Fig. 1, respectively. In Case 1, the backfill surface ground motion was recorded at the seismic monitoring station of the Korea Institute of Ocean Science and Technology, which was installed on the backfill surface of the damaged wall [41]. In Cases 2–8, the acceleration time histories on the ground surface were obtained by Fukunaga et al. [15], who performed a one-dimensional site response analysis on the bedrock ground motion measured at the seismic monitoring station of the nationwide strong-motion network (K-NET) closest to the damaged wall [29]. Either the north–south (N-S) or east–

Table 3 Details of the eight datasets used in quantitative evaluations [29, 41]

| Case no. | Earthquake name | Year | Magnitude (M _w) | Station | Location | | Distance from epicenter (km) | Port name | H _v (m) | T _b (s) | T _a (s) | a _{cr} (g) | Average measured D _h (m) | b |
|----------|----------------------|------|-----------------------------|---------------|----------|--------|------------------------------|-------------|--------------------|--------------------|--------------------|---------------------|-------------------------------------|------|
| | | | | | E | W | | | | | | | | |
| 1 | Pohang | 2017 | 5.4 | ORPHT | 129.262 | 36.064 | 6.000 | Youngil Bay | 15.6 | 0.237 | 0.052 | 0.147 | 0.05 | 0.73 |
| 2 | Tokachi-Oki | 1968 | 8.2 | Muroran-S | 140.968 | 42.337 | 1.537 | Muroran | 10.6 | 0.857 | 0.597 | 0.108 | 0.122 | 0.86 |
| 3 | Tohoku-Pacific Ocean | 2011 | 9.0 | Onahamaji-G | 140.874 | 36.929 | 3.852 | Onahama | 15.7 | 0.374 | 0 | 0.134 | 0.225 | 0.71 |
| 4 | Sanriku-Haruka-Oki | 1994 | 7.7 | Hachinoheji-S | 140.759 | 40.834 | 0.940 | Hachinohe | 17.6 | 0.311 | 0 | 0.128 | 0.072 | 0.78 |
| 5 | Kushiro-Oki | 1993 | 7.8 | Kushiro-G | 144.363 | 42.994 | 0.842 | Kushiro | 6.5 | 0.226 | 0.071 | 0.126 | 0.1 | 0.34 |
| 6 | Hokkaido-Toho-Oki | 1994 | 8.3 | Hanasaki-F | 145.581 | 43.286 | 0.496 | Nemuro | 4.3 | 0.378 | 0.295 | 0.144 | 0.054 | 0.36 |
| 7 | Hokkaido-Toho-Oki | 1994 | 8.3 | Hanasaki-F | 145.579 | 43.285 | 0.61 | Nemuro | 6.9 | 0.167 | 0.007 | 0.099 | 0.119 | 0.36 |
| 8 | Hokkaido-Toho-Oki | 1994 | 8.3 | Hanasaki-F | 145.566 | 43.280 | 1.639 | Nemuro | 7.5 | 0.113 | 0 | 0.109 | 0.06 | 0.38 |

west (E-W) direction was used for the motions, depending on the direction that was closest to the perpendicular of the damaged wall.

The D_h prediction accuracy of the proposed analysis methods for the performance-based design was quantitatively evaluated according to the following process:

- (1) The MP values included in the proposed methods were derived from the motions illustrated in Fig. 1, as summarized in Table 4.
- (2) D_h was calculated for each event by substituting the a_{cr} values in Table 3 and MP values in Table 4 into the proposed simplified dynamic analysis methods (listed in Table 2) and the k_{hk} concept (Eq. 3). Here, the values of D_h calculated from the k_{hk} concept refer to the D_a values derived by substituting the terms k_{hk} , a_c , and D_r in Eq. 3 with the a_{cr} values in Table 3 divided by g , a_c values in Table 4, and D_r value of 10 cm, respectively [15, 32, 44].
- (3) The calculated D_h values were then compared with the measured D_h values of the actual damage cases summarized in Table 3. The relative difference (RD) in percentage between the measured and calculated D_h values is plotted in Fig. 2 for all cases. To facilitate the analysis of the cause of the RD, this figure also presents the major MP values (i.e., PGA, PGV, T_p , I_a , a_{cr}/PGA , and PGV/PGA) for all cases.

The eight cases are arranged in ascending order of the RD values. An RD converging to 0 indicates a high prediction accuracy, whereas negative and positive values indicate that the method underestimated or overestimated D_h , respectively. The analysis results were divided into three groups: Group 1 (i.e., upper bound [3, 9, 47, 53]), Group 2 (i.e., mean fit [61, 62]), and the k_{hk} concept.

The PGA is the most commonly used measure for the amplitude of a particular ground motion. Figure 2 indicates that the RD values of Groups 1 and 2 increased as PGA increased. The ratio a_{cr}/PGA is a key parameter of simplified dynamic analysis methods; the RD values of Groups 1 and 2 increased as a_{cr}/PGA decreased. In the case of Group 1, the absolute value of RD decreased as PGA increased up to 0.3 g and a_{cr}/PGA decreased up to 0.44. Meanwhile, D_h was gradually overestimated as PGA increased above 0.3 g and a_{cr}/PGA decreased below 0.44. In the case of Group 2, the absolute value of RD decreased as PGA increased and a_{cr}/PGA decreased, but D_h was underestimated overall. The predominant period (T_p) [52] and the ratio of PGV/PGA [56] are the MP reflecting the frequency content characteristics of the ground motion [30]. As they decreased, the RD values of each group exhibited the same trends with increasing PGA and decreasing a_{cr}/PGA . The Arias intensity (I_a) [5] represents the characteristic of the ground motion duration; Case 5

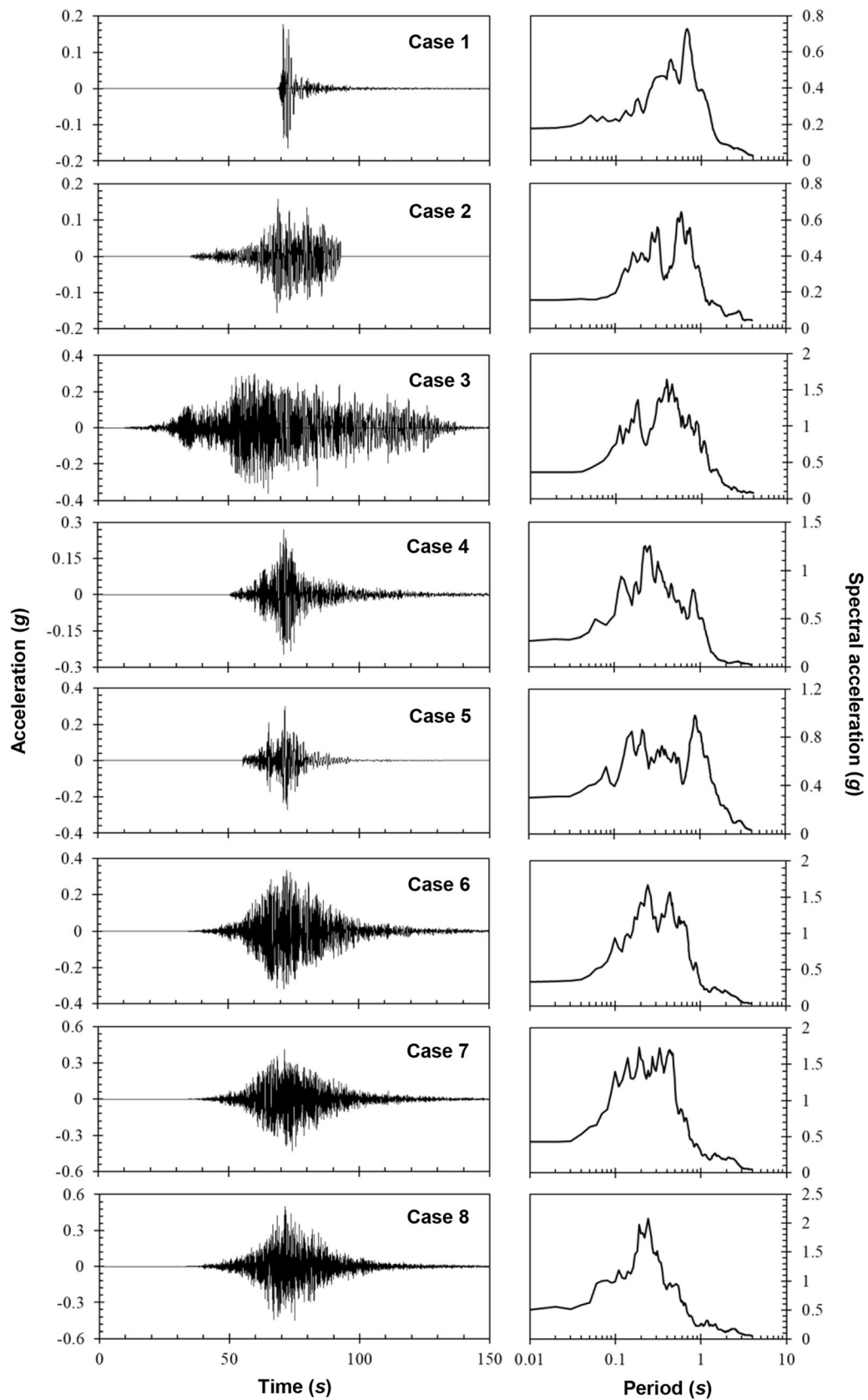


Fig. 1 Acceleration time histories and response spectra at the backfill surface of the eight datasets [15, 41]

Table 4 MP values of the acceleration time histories at the backfill surface in the eight datasets

| Case no. | PGA (g) | PGV (m/s) | PGD* (m) | T_p (s)** | I_a *** (m/s) | a_f (g) | a_c (g) |
|----------|---------|-----------|----------|-------------|-----------------|-----------|-----------|
| 1 | 0.178 | 0.159 | 0.028 | 0.68 | 0.377 | 0.099 | 0.051 |
| 2 | 0.157 | 0.142 | 0.020 | 0.59 | 1.138 | 0.076 | 0.055 |
| 3 | 0.302 | 0.324 | 0.047 | 0.39 | 15.46 | 0.115 | 0.105 |
| 4 | 0.272 | 0.273 | 0.032 | 0.23 | 2.249 | 0.101 | 0.054 |
| 5 | 0.271 | 0.314 | 0.057 | 0.88 | 1.838 | 0.067 | 0.041 |
| 6 | 0.334 | 0.289 | 0.034 | 0.24 | 8.459 | 0.053 | 0.041 |
| 7 | 0.414 | 0.266 | 0.030 | 0.19 | 10.60 | 0.053 | 0.038 |
| 8 | 0.503 | 0.257 | 0.027 | 0.24 | 9.236 | 0.042 | 0.032 |

*Peak ground displacement

**Predominant period [52]

***Arias intensity [5]

was exceptional because I_a was so small that it resulted in a relatively small D_h . The analysis results indicated that the simplified dynamic analysis methods were partially reliable when the MP values in the equations were within a certain range. Therefore, to accurately predict earthquake-induced D_h under various external conditions, simplified dynamic analysis methods should include the appropriate MP by considering the frequency characteristics and duration of the ground motion in their equations [8, 12, 16, 24, 30, 44].

The k_{hk} concept corrects the frequency characteristics and duration of the ground motion through the b filter and P , respectively. Thus, in most cases, it provided a better prediction accuracy of D_h than the simplified dynamic analysis methods. However, the k_{hk} concept was confirmed to predict D_h relatively conservatively in cases where the long-period components of the ground motion were dominant. This is similar to the results of Lee et al. [32], who verified the reliability of the k_{hk} concept through dynamic centrifuge tests. Therefore, the terms related to the low-frequency band should be improved for the design of the b filter.

2.2 Overview of the dynamic centrifuge tests performed by Lee et al. [32]

Centrifuge tests rotate a scaled model at high speed with a centrifugal acceleration far higher than that of gravity and can be used to simulate in situ stress conditions in soil models. They have been used in many prior studies to supplement the lack of recorded case histories to validate the reliability of existing design methods [6, 31, 33, 35, 45, 48, 59, 63] and develop seismic design techniques for port structures [11, 19, 31, 33, 63]. Several performance-based seismic design codes for port structures have recently recommended centrifuge testing as a seismic performance verification method [4, 22, 38, 40]. In this

study, the dynamic centrifuge test results of Lee et al. [32] were used to quantitatively evaluate the proposed simplified dynamic analysis methods and the k_{hk} concept as well as to improve the b filter.

Lee et al. [32] performed four dynamic centrifuge tests on gravity-type quay wall models subjected to various conditions reflecting the primary variables of the k_{hk} concept (i.e., H_w , the thickness of the subsoil underneath the wall (H_u), and input earthquake motion) in order to validate the k_{hk} concept and assess the behavior of the model walls during earthquakes. Each of these test cases is summarized in Table 5. The effects of H_w , H_u , and the frequency characteristics of the input earthquake on the accuracy of predicting D_h using the k_{hk} equation were evaluated by comparing the results of Cases 1 and 2, Cases 2 and 3, and Cases 3 and 4, respectively. The tests were conducted at KAIST with an earthquake simulator mounted on the centrifuge [26, 27]. An equivalent shear beam (ESB) box, which minimized the boundary effect on the soil, was used as a model container [34]. The gravity-type quay wall models were made from aluminum alloy (T6061) and designed with $k_{hk} = 0.13$ based on the quay wall design procedure provided by MLIT [38]. The subsoil underneath the wall and the backfill soil behind the wall were constructed from poorly graded clean silica sandy soil (SP). The physical properties of the sand were reported by Lee et al. [32]. The subsoil was densified to a relative density of 86% by compaction to prevent overturning and bearing capacity failure. The soil in the backfill was prepared by sand pluviation at a relative density of 80%. Figure 3a shows the configurations of the test models with instrumentation for Cases 1 and 2, and Fig. 3b shows the configurations for Cases 3 and 4.

In Cases 1 and 2, there were three pairs of bender elements, and in Cases 3 and 4, there were four pairs of bender elements. T_u and T_b were obtained by measuring the shear

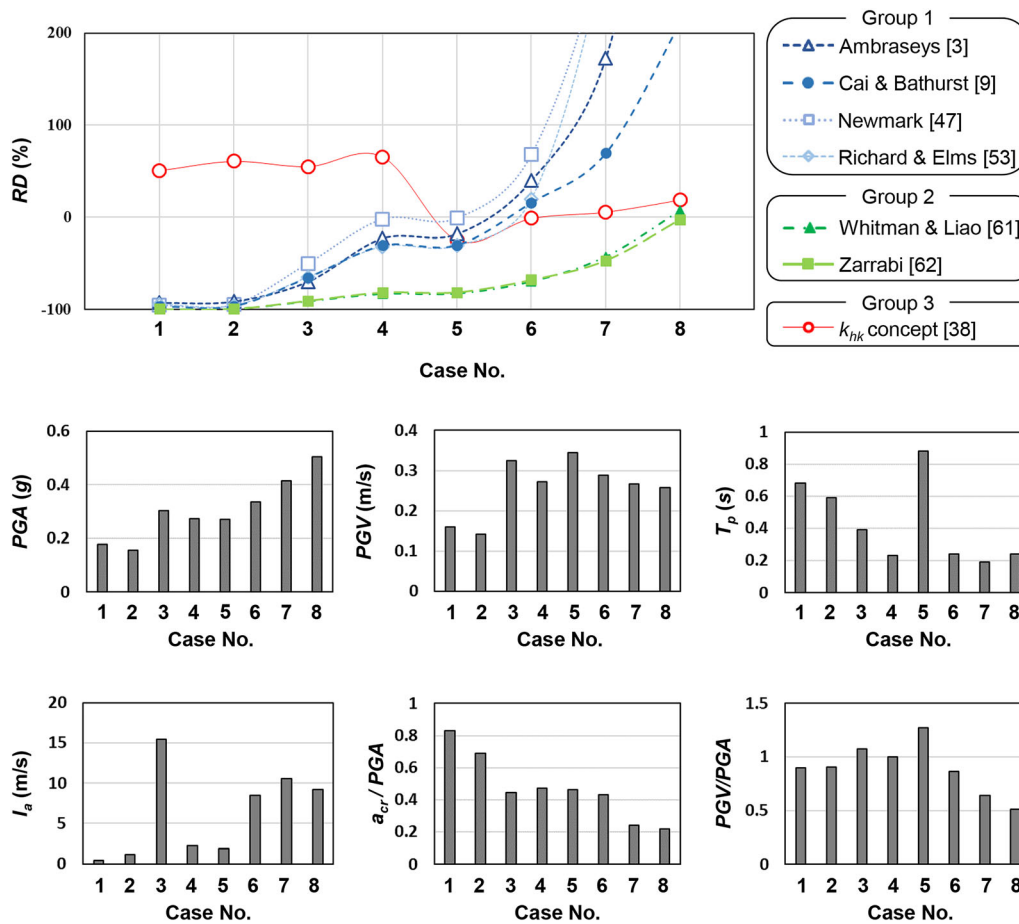


Fig. 2 Relative difference in percentage between the measured and calculated D_h values and the major MP values for all cases

wave velocity (V_s) of models in flight. An accelerometer was attached to the bottom part of the ESB box parallel to the shaking direction to measure the input motion. Five of the eight horizontal accelerometers were buried in the soil, and the rest were attached to the model wall to measure the acceleration time histories at different soil heights and the gravity-type quay wall. D_h was measured with two potentiometers. Two laser sensors were used to measure the subsidence of the backfill and to check the bearing capacity failure of subsoil based on the settlement of the wall. The acceleration and D_h were positive in the active direction. The Ofunato earthquake motion recorded at Miyagi-Ken Oki, Japan, which has short-period components, and the Hachinohe earthquake motion recorded at Tokachi-Oki, Japan, which has long-period components, were used as the shaking events. Figure 4 presents the acceleration time histories and the response spectra of the input motions. The dynamic motions were inputted incrementally at the bottom of the ESB, beginning with a weak intensity. The centrifugal acceleration was set to 40 g for the 10 m high wall and 60 g for the 15 m high wall. All results presented herein are in prototype units unless otherwise stated

according to the centrifuge scaling laws [55]. The details of the dynamic centrifuge tests are available in the paper by Lee et al. [32].

3 Results and discussion

3.1 Assessment of the simplified dynamic analysis methods and k_{hk} concept with the centrifuge test results

Similar to the analysis presented in Sect. 2.1, Lee et al. [32] evaluated the prediction accuracy of the k_{hk} concept at estimating D_h after the force balance limit was reached under various conditions (i.e., H_w , H_u , and earthquake input motion) by comparing the D_h values measured via the centrifuge tests with those calculated from a_c based on the k_{hk} definition. This section presents a quantitative evaluation of the accuracy of the simplified dynamic analysis methods using the centrifuge test results. The process used was the same as that described in Sect. 2.1, except that the

Table 5 Overview of the test cases (modified from Lee et al. [32])

| | | Case 1 | Case 2 | Case 3 | Case 4 |
|--------------------------|--|-------------------------|---------|---------|---------|
| Wall model information | H_w (m) | 10 | 15 | 15 | 15 |
| | Width (m) | 5.68 | 8.52 | 8.52 | 8.52 |
| | Length* (m) | 19.48 | 29.22 | 29.22 | 29.22 |
| | Weight (ton) | 580 | 1960 | 1960 | 1960 |
| Soil model information | H_u (m) | 2.4 | 2.4 | 13 | 13 |
| | T_u (s) | 0.057 | 0.078 | 0.210 | 0.220 |
| | T_b (s) | 0.342 | 0.467 | 0.580 | 0.610 |
| | Relative density of subsoil (%) | 86 | 86 | 86 | 86 |
| | Relative density of backfill (%) | 80 | 80 | 80 | 80 |
| | Internal friction angle of subsoil (°) | 43.7 | 43.7 | 43.7 | 43.7 |
| | Internal friction angle of backfill (°) | 43 | 43 | 43 | 43 |
| | Input motion information | Earthquake input motion | Ofunato | Ofunato | Ofunato |
| Supplemental information | T_p | 0.249 | 0.249 | 0.249 | 0.337 |
| | T_o^{**} | 0.359 | 0.359 | 0.359 | 0.666 |
| | T_m^{**} | 0.377 | 0.377 | 0.377 | 0.724 |
| | b value | 0.48 | 0.68 | 0.68 | 0.69 |
| | Inter-friction angle between model wall and subsoil (°) | 29 | 29 | 29 | 29 |
| | Inter-friction angle between model wall and backfill (°) | 21.5 | 21.5 | 21.5 | 21.5 |

* All walls spanned the length of the container (i.e., 487 mm at the model scale, which was 2 mm less than the length of the container to eliminate friction)

** T_o : smoothed spectral predominant period; T_m : mean period [52]

dynamic centrifuge test results were used instead of actual records of earthquake-damaged quay walls.

For each earthquake excitation, the acceleration time histories at the bedrock and soil and the displacement time histories of the wall were measured to deduce the MP values used to calculate D_h . Then, the actual D_h was obtained by subtracting the average value of the initial 500

samples from the average value of the last 500 samples from the displacement time histories. The deduced MP values (i.e., PGA, PGV, a_f and a_c) and the calculated D_h for all seismic events in every case are plotted with respect to the measured D_h in Figs. 5 and 6.

As summarized in Table 5, each case had different combinations of H_w , H_u , and input earthquake motions so

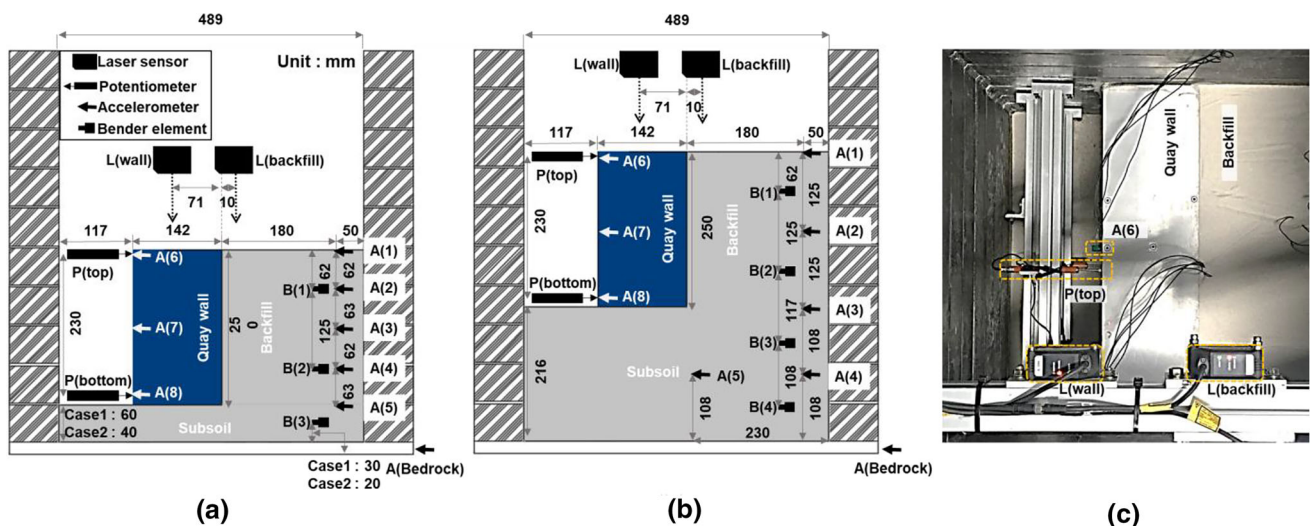


Fig. 3 Schematic of the test instrumentation (all dimensions are in model scale): **a** Cases 1 and 2, **b** Cases 3 and 4, and **c** top view for Case 1 (modified from Lee et al. [32])

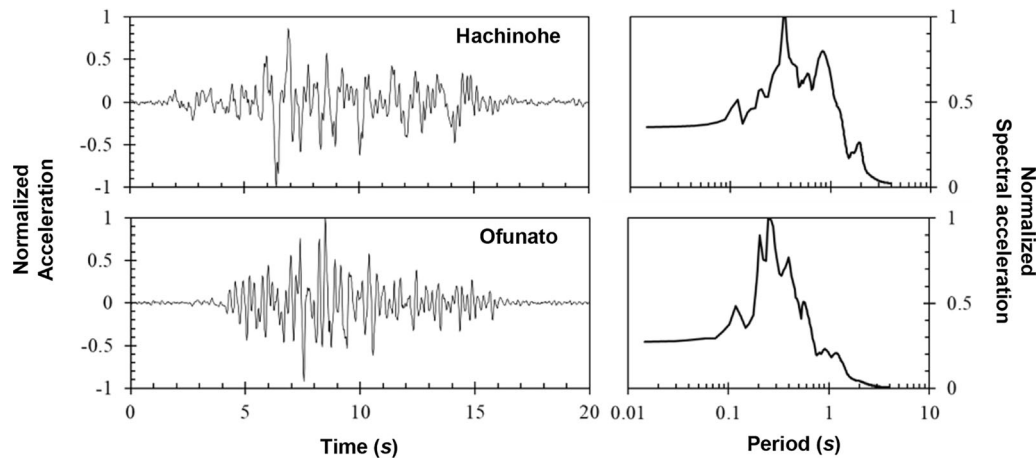


Fig. 4 Normalized acceleration time histories and response spectra of input motions to the earthquake simulator during the centrifuge tests at the prototype scale (modified from Lee et al. [32])

that the average values of T_p obtained from the acceleration time histories on the backfill surface of each case were 0.15, 0.26, 0.55, and 0.60 s. As in Sect. 2.1, the analysis results were divided into three groups: Group 1 (i.e., upper bound [3, 9, 47, 53]), Group 2 (i.e., Mean fit [61, 62]), and the k_{hk} concept. In the case of Group 1, Fig. 6 indicates that the calculated D_h values were larger than the measured D_h values for Cases 1–3, and the difference between the calculated and measured D_h gradually decreased as the average T_p increased. The calculated D_h values were less than the measured D_h values in Case 4, which had the longest T_p in the test model. In the case of Group 2, the calculated D_h values were only larger than the measured D_h values for Case 1, which had the shortest T_p in the test model. In Cases 2–4, Group 2 increasingly underestimated D_h with increasing T_p . Finally, the k_{hk} concept slightly overestimated D_h in all cases, but it generally had a higher prediction accuracy than the other methods because it also considered the effects of external factors (e.g., wall geometry, stiffness of soil, and the frequency characteristics and duration of the ground motion). However, because the difference between the calculated and measured D_h increased for cases with more low-frequency components, the terms of the b filter related to the low-frequency band should be improved.

3.2 Time–frequency domain responses of the wall models

The analyses in Sects. 2.1 and 3.1 confirmed that the k_{hk} concept had a higher D_h prediction accuracy than the simplified dynamic analysis methods under various external conditions. This is because the k_{hk} concept adopts the b filter that corrects the frequency characteristics of the ground motion by considering the contribution of the

waves of each frequency component comprising the ground motion to the D_h generation. Nagao and Iwata [44] confirmed through numerical analysis that the frequency components below 1 Hz of ground motion are mainly related to D_h generation and suggested the b filter (Eq. 1). In the present study, a time–frequency analysis was performed with the dynamic centrifuge test results to evaluate the suitability of the b filter shape experimentally. Time–frequency analysis is an effective method of investigating the changing frequency content of the dynamic response over time [46, 51, 59]. The dynamic displacement of the wall models was obtained by double integration of the acceleration signals measured from the accelerometer, which was attached to the top of the wall front (A(6) in Fig. 3). Figures 7 and 8 present the time histories of the dynamic displacement and permanent displacement, the frequency contents of the dynamic displacement, and the time–frequency domain of the dynamic response for the wall models of all cases during a weak earthquake (i.e., PGA at backfill surface, $A(6) \cong 0.1 g$) and a strong earthquake (i.e., PGA at backfill surface, $A(6) \cong 0.3 g$), respectively. The frequency energy of the dynamic response of the wall model was concentrated at 1 Hz or less in all cases. In particular, the permanent displacement occurred where the frequency energy below 1 Hz was dominant in all cases. Because the frequency components below 1 Hz were the main contributors to D_h generation, the suitability of b filter shape was experimentally reconfirmed. The results in Sects. 2.1 and 3.1 indicate that the k_{hk} concept generally predicts D_h reasonably well after the force balance limit is reached but is less accurate in cases containing many low-frequency components. To improve the performance, b (Eqs. 1c and 1d) was revised according to the dynamic centrifuge test results and actual cases of earthquake-damaged quay walls.

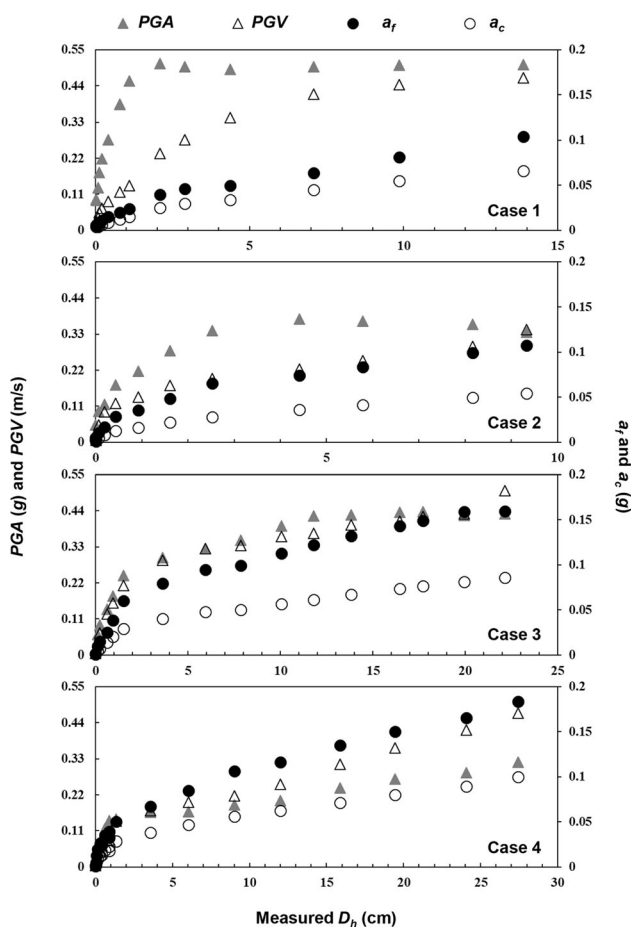


Fig. 5 MP values of the acceleration time histories at the backfill surface with respect to the measured D_h values for all seismic events in every case (modified from Lee et al. [32])

3.3 Revision of b using the centrifuge test results

Equations 1c and 1d were derived by multiple linear regression analysis of the correlation between the three independent variables of H , T_b , and T_u and the dependent variable of b based on the numerical analysis introduced by Nagao and Iwata [44].

To perform multiple linear regression analysis with the centrifuge test results, the target b values (b_{target}) corresponding to the values of D_h measured from the dynamic centrifuge tests were derived. Here, b_{target} represents the b value that makes a_c from the measured acceleration time history produce the measured D_h of gravity-type quay wall models designed with $k_{hk} = 0.13$. Multiple linear regression analysis was performed using events where the measured D_h value was close to 5–20 cm, which is the applicable range of k_{hk} .

Figure 9 details the procedure for obtaining b_{target} using the measured signals in the centrifuge tests. The signals were obtained for Case 4, where the Hachinohe earthquake

with PGA at the backfill surface equal to 0.2 g was applied to the test model.

- (1) During each earthquake excitation, the acceleration time history of the backfill soil surface (A(1)) and the displacement time history of the wall (P(top)) were obtained.
- (2) The a_c value corresponding to each D_h ($a_{c, target}$) was deduced by substituting the design k_{hk} value of 0.13 for the quay wall model and the measured D_h values into the k_{hk} and D_a terms of Eq. 3.
- (3) To design the filter, b was initially set to 0.01. The filters for all seismic events were designed by using b and frequency characteristics of the measured acceleration time histories; the designed filters were applied to the acceleration spectra obtained by the FFT of the measured acceleration time histories.
- (4) The filtered acceleration time histories were obtained by the inverse FFT operation on the filtered acceleration spectra. Then, a_f and P were derived from the filtered acceleration time histories and multiplied with each other to calculate a_c ($a_{c, calculation}$), which was then compared with $a_{c, target}$.
- (5) Steps 3 and 4 were repeated while b was increased from 0.01 to 1.5 in steps of 0.01, and the b value with the smallest error between $a_{c, target}$ and $a_{c, calculation}$ was found (b_{target}). Here, $a_{c, calculation}$ should be equal to or greater than $a_{c, target}$.

The measured D_h , $a_{c, target}$, b_{target} , T_b , and T_u values of the events for each case are summarized in Table 6. For the multiple linear regression analysis, the independent variables needed to be determined first. Various studies [20, 21, 43], including the results of the dynamic centrifuge test [32] and numerical analysis [44], confirmed that the low-frequency components of an earthquake motion in backfill soil become more amplified with increasing T_b , and a greater D_h is generated. Therefore, in order for the calculated b to increase with the amplification of low-frequency components in the backfill soil, the coefficients of the independent variables H_w , T_b , and T_u should be positive. However, in Eq. 3, the coefficients of H_w and T_u are positive whereas that of T_b is negative. According to Nagao and Iwata [44], there is no physical basis for estimating the coefficient of T_b to be negative, and this was merely done to improve the accuracy of the equation. In particular, because T_b represents a natural period that includes not only the backfill but also the subsoil, Eq. 3 considers T_u redundantly. Therefore, a multiple linear regression analysis was performed on b with H_w , T_b , and T_u as the independent variables. Then, additional analysis was conducted with only H_w and T_b as the independent variables. Following Nagao and Iwata [44], the reference values of H_w ,

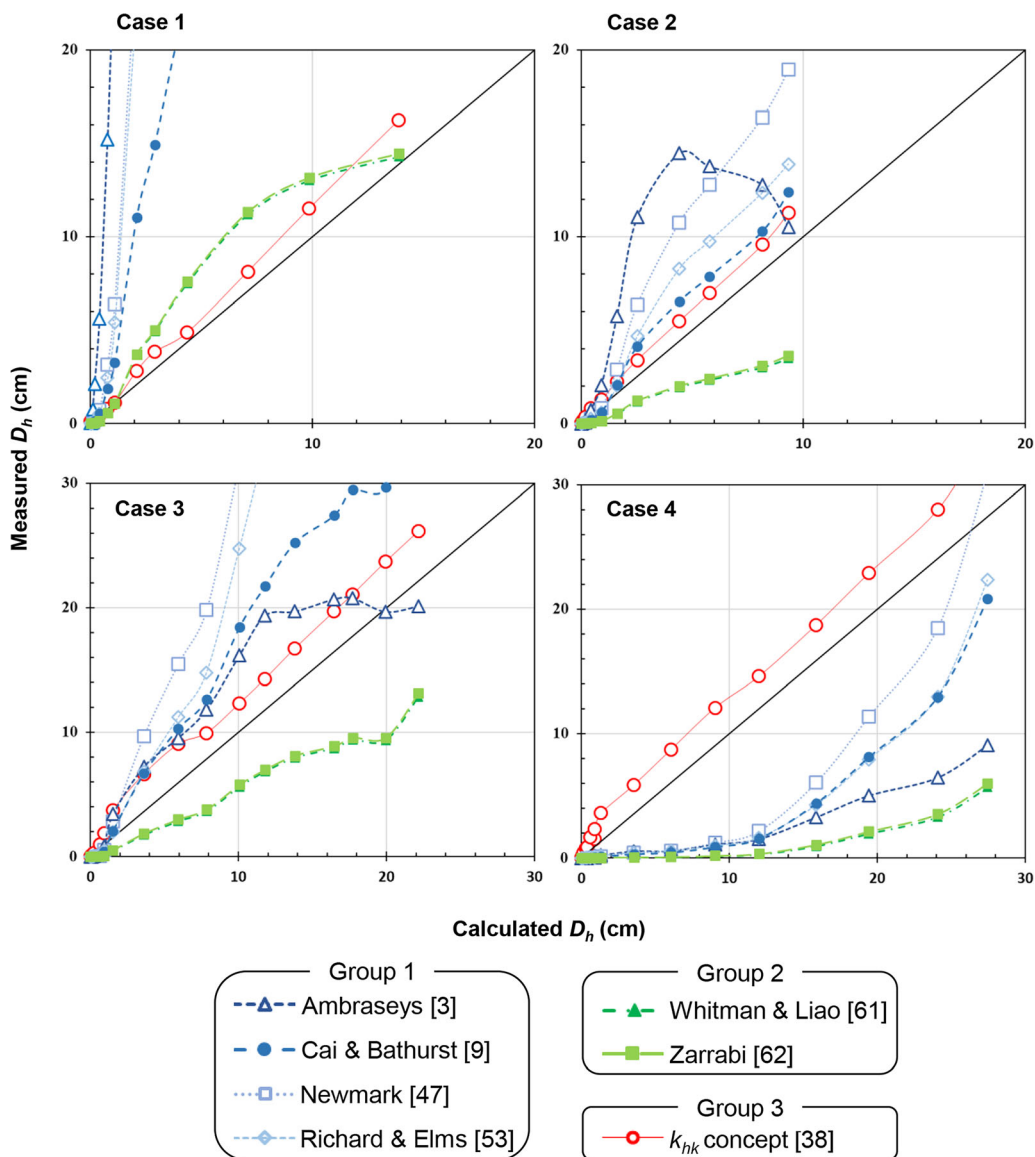


Fig. 6 Comparison of the calculated and measured D_h values for all cases

T_b , and T_u were set to 15 m, 0.8 s, and 0.4 s, respectively, for non-dimensionalization and normalization.

Through the multiple linear regression analysis, the following Eqs. 4 and 5 were derived. The adjusted R squared values, which indicated the suitability of the regression model, were 0.96 and 0.97, respectively.

$$b_1 = 0.13 \frac{H_w}{H_{wR}} + 0.37 \frac{T_b}{T_{bR}} - 0.06 \frac{T_u}{T_{uR}} + 0.24 \tag{4}$$

$$b_2 = 0.18 \frac{H_w}{H_{wR}} + 0.26 \frac{T_b}{T_{bR}} + 0.25 \tag{5}$$

Here, H_w is the wall height (m), H_{wR} is the standard wall height (15 m), T_b is the initial natural period of the backfill ground (s), T_{bR} is the standard initial natural period of the backfill ground (0.8 s), T_u is the initial natural period of the

subsoil underneath the wall (s), and T_{uR} is the standard initial natural period of the subsoil underneath the wall (0.4 s).

The adjusted R squared values indicate that the suitability of b_2 (Eq. 5), which excludes T_u as an independent variable, was the same or greater than that of b_1 (Eq. 4), which does include T_u . In addition to the adjusted R squared values, the D_h values derived with Eqs. 4 and 5 were compared with the measured D_h values to evaluate the prediction accuracy. The results are presented in Fig. 10. Applying the revised b values (Eqs. 4 and 5) to obtain a_c for calculating k_{hk} decreased the difference between the calculated and measured D_h values for all cases, compared to the original b value (Eqs. 1c and 1d). The revised b values considerably improved the D_h

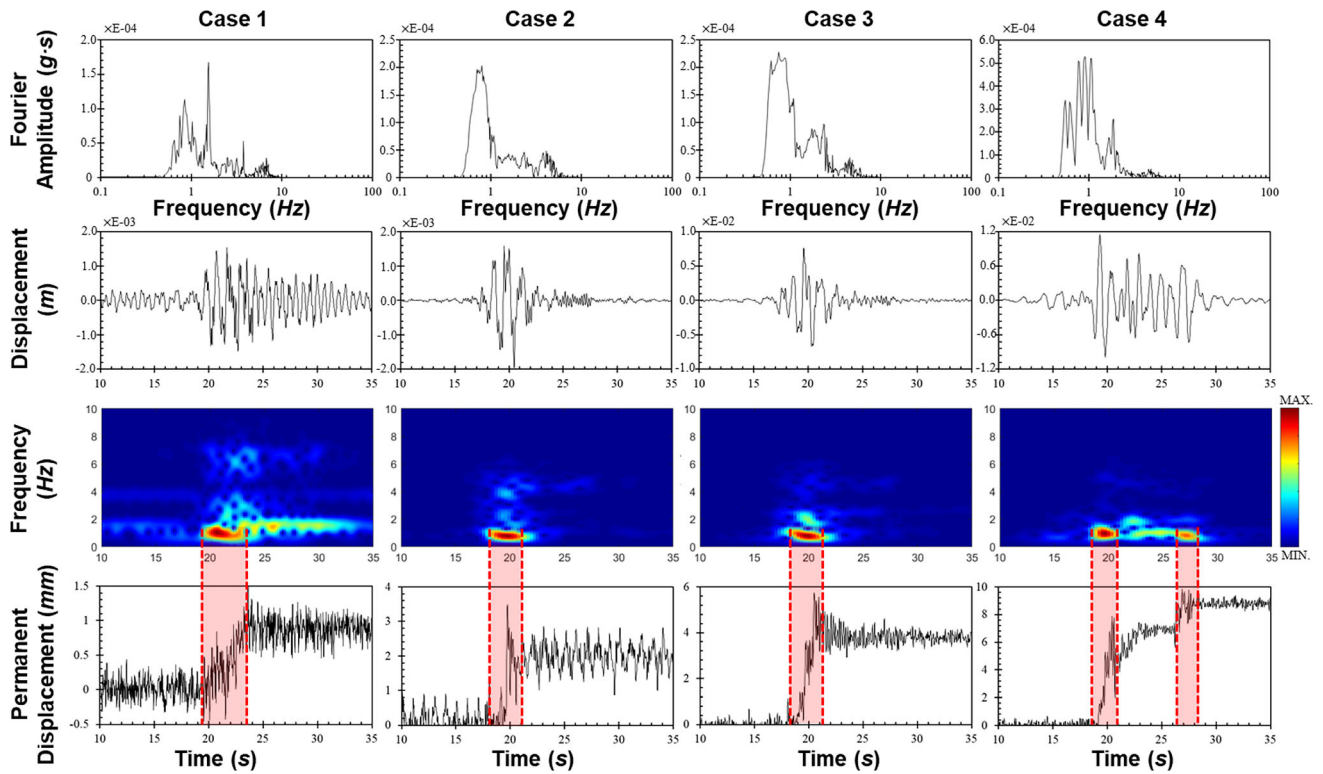


Fig. 7 Frequency contents of the dynamic displacement, time histories of the dynamic and permanent displacements, and time–frequency domain of the dynamic response for the wall models of all cases during the weak earthquake (PGA at backfill surface, $A(1) \cong 0.1 g$)

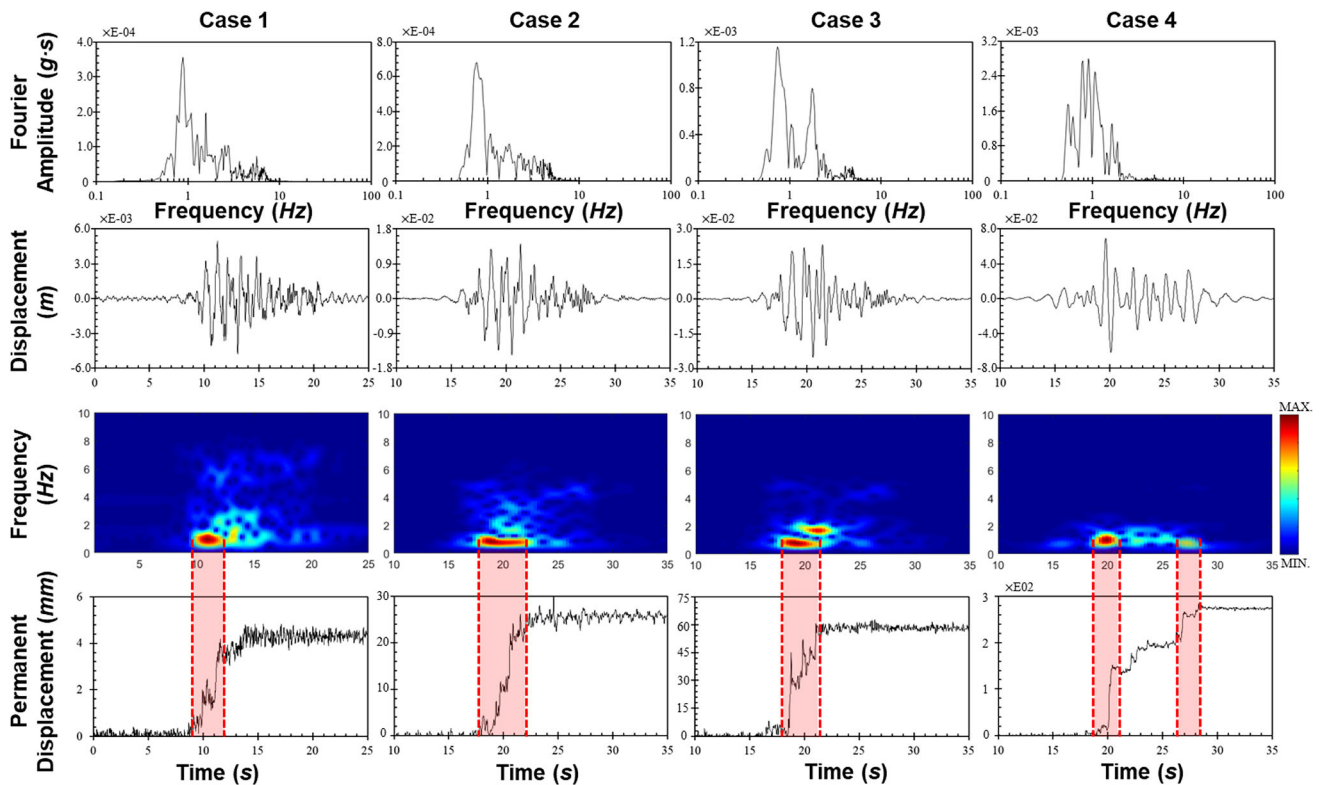


Fig. 8 Frequency contents of the dynamic displacement, time histories of the dynamic and permanent displacements, and time–frequency domain of the dynamic response for the wall models of all cases during the strong earthquake (PGA at backfill surface, $A(1) \cong 0.3 g$)

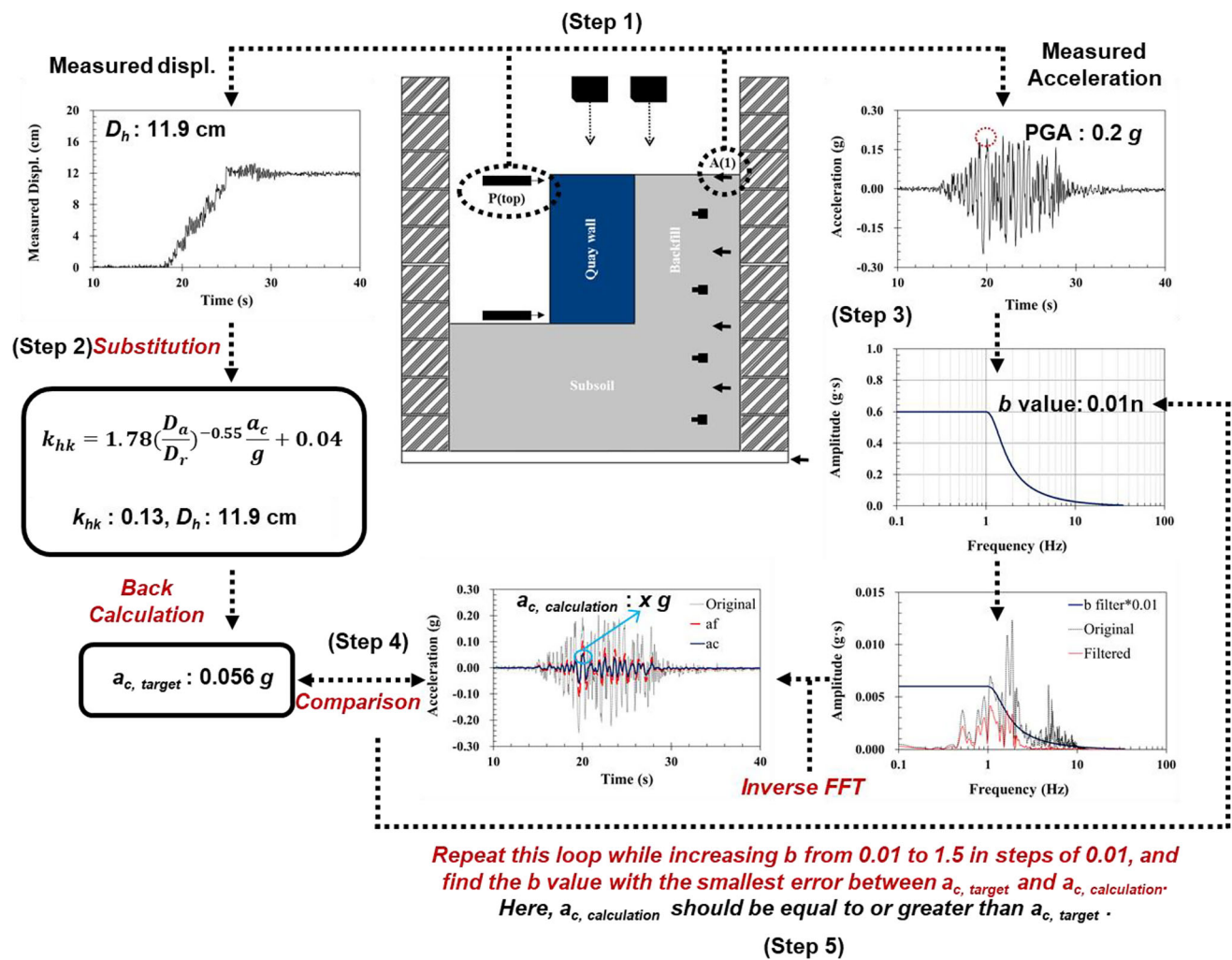


Fig. 9 Procedure for obtaining b_{target} from the measured signals

prediction accuracy for Cases 3 and 4, which included more low-frequency components, compared to Cases 1 and 2. In Cases 3 and 4, the D_h values calculated with b_1 (Eq. 4) were slightly less than the measured D_h values, which means that Eq. 4 can cause k_{hk} to be underestimated. These results suggest that b_2 (Eq. 5) is more suitable than b_1 (Eq. 4) for calculating k_{hk} with regard to simplicity and safety.

Because the reliability of the revised b values (Eqs. 4 and 5) was evaluated with the dynamic centrifuge test results used to derive the two equations, it is natural for the results to be positive. Therefore, further verification using actual cases of earthquake-damaged quay walls was required to confirm the field applicability and reliability of the revised b values (Eqs. 4 and 5).

3.4 Assessment of the revised b values using actual cases of earthquake-damaged quay walls

The procedure and actual records of earthquake-damaged quay walls presented in Sect. 2.1 were applied to validate the field applicability and reliability of the revised b values (Eqs. 4 and 5). RD was determined between the calculated D_h values obtained with the different b values (Eqs. 1c, 1d, 4, and 5) and the measured D_h values summarized in Table 3. The calculated D_h values were obtained by substituting the a_{cr} values in Table 3 and the a_c values derived from the different b values (Eqs. 1c, 1d, 4, and 5) into the real earthquake records in Fig. 1 into the k_{hk} and a_c terms of Eq. 3. The revised b values for all cases used in the evaluation and the corresponding a_c values are summarized in Table 7. The RD values for all cases are plotted in Fig. 11.

Table 6 Measured D_h , $a_{c, target}$, b_{target} , T_b , and T_u values for the events of each case used in the multiple linear regression analysis

| Case no. | Event no. | Measured D_h (cm) | $a_{c, target}$ (g) | b_{target} | T_b (s) | T_u (s) |
|----------|-----------|---------------------|---------------------|--------------|-----------|-----------|
| 1 | 11 | 4.37 | 0.032 | 0.46 | 0.330 | 0.055 |
| | 12 | 7.09 | 0.042 | 0.47 | 0.340 | 0.056 |
| | 13 | 9.86 | 0.050 | 0.48 | 0.342 | 0.057 |
| | 14 | 13.89 | 0.061 | 0.48 | 0.340 | 0.059 |
| 2 | 10 | 4.41 | 0.032 | 0.57 | 0.465 | 0.075 |
| | 11 | 5.78 | 0.037 | 0.56 | 0.462 | 0.069 |
| | 12 | 8.16 | 0.045 | 0.58 | 0.467 | 0.078 |
| | 13 | 9.33 | 0.049 | 0.59 | 0.470 | 0.079 |
| 3 | 8 | 5.94 | 0.038 | 0.59 | 0.570 | 0.195 |
| | 9 | 7.85 | 0.044 | 0.60 | 0.580 | 0.200 |
| | 10 | 10.07 | 0.051 | 0.61 | 0.590 | 0.210 |
| | 11 | 11.79 | 0.055 | 0.60 | 0.581 | 0.200 |
| | 12 | 13.82 | 0.060 | 0.60 | 0.580 | 0.200 |
| | 13 | 16.47 | 0.067 | 0.59 | 0.570 | 0.195 |
| | 14 | 17.71 | 0.069 | 0.60 | 0.580 | 0.200 |
| | 15 | 19.94 | 0.074 | 0.61 | 0.590 | 0.210 |
| 4 | 16 | 22.15 | 0.078 | 0.60 | 0.581 | 0.200 |
| | 10 | 3.55 | 0.029 | 0.61 | 0.595 | 0.220 |
| | 11 | 6.05 | 0.038 | 0.62 | 0.600 | 0.222 |
| | 12 | 9.03 | 0.048 | 0.63 | 0.610 | 0.240 |
| | 13 | 11.99 | 0.056 | 0.62 | 0.610 | 0.210 |
| | 14 | 15.87 | 0.065 | 0.62 | 0.600 | 0.222 |
| | 15 | 19.43 | 0.073 | 0.61 | 0.595 | 0.220 |
| | 16 | 24.07 | 0.082 | 0.62 | 0.600 | 0.222 |
| | 17 | 27.44 | 0.088 | 0.63 | 0.610 | 0.240 |

Similar to the evaluation in Sect. 3.3 with the dynamic centrifuge test results, Fig. 11 indicates that the revised b values (Eqs. 4 and 5) significantly improved the accuracy of the calculated D_h values, compared to the original b values (Eqs. 1c and 1d) in Cases 1–4, which contained more low-frequency components. In cases 5–7, where H_w was less than 7 m, using the revised b values caused D_h to be calculated slightly conservatively compared to when the original b values were used (Eqs. 1c and 1d). Particularly in case 5, using the original b values caused the calculated D_h to underestimate the measured D_h , but applying the revised b values (Eqs. 4 and 5) allowed D_h to be safely predicted. In addition, the variation in RD was confirmed to be small when the revised b values were used instead of the original b values. Thus, the revised b values (Eqs. 4 and 5) allowed D_h to be predicted consistently, regardless of external influences (e.g., H_w , T_b , earthquake motions).

The field applicability and reliability of the revised b values (Eqs. 4 and 5) were partially verified through the above evaluation using actual cases of earthquake-damaged quay walls. Because the RD values with b_1 (Eq. 4)

and b_2 (Eq. 5) were similar, the better equation cannot be quantitatively determined. However, in terms of the simplicity of the equation and verification with the centrifuge test results in Sect. 3.3, Eq. 5 comprising the independent variables H_w and T_b can be concluded to be more effective.

4 Conclusions

This study assessed representative simplified dynamic analysis methods and the k_{hk} concept for the performance-based design of port structures. Incident records of earthquake-induced damage on quay walls in Japan and Korea and the results of dynamic centrifuge tests performed under various conditions were used for a quantitative evaluation and improvements. Unlike the simplified dynamic analysis methods, which simply reflect the frequency characteristics of the ground motion associated with the deformation of the quay wall as the ratio of PGV to PGA, the k_{hk} concept corrects the frequency characteristics of the ground motion by also considering the wall geometry, stiffness of the soil,

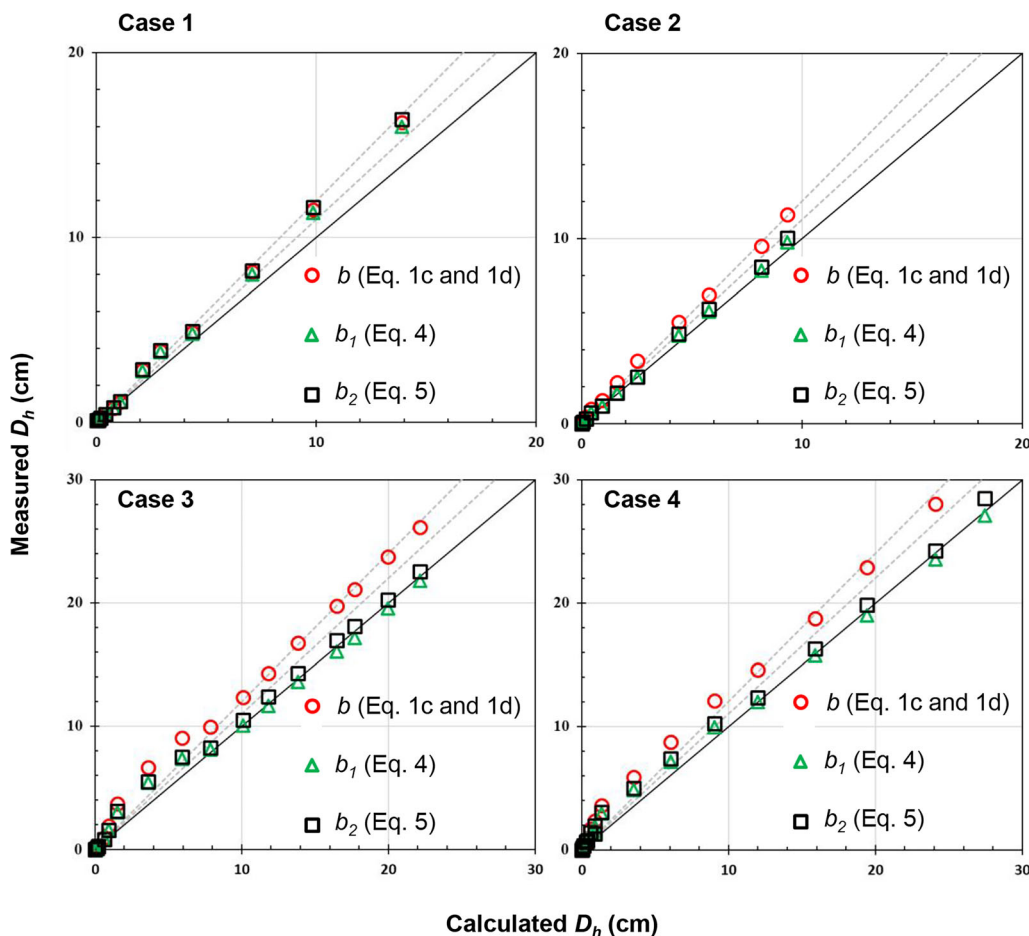


Fig. 10 Comparison between the D_h values calculated with a_c filtered by b (Eqs. 1c and 1d), b_1 (Eq. 4), and b_2 (Eq. 5) and the measured D_h values for all cases

Table 7 Revised b values (Eqs. 4 and 5) for all cases and the corresponding a_c values

| Case no. | b_1 | a_c with b_1 (g) | b_2 | a_c with b_2 (g) |
|----------|-------|----------------------|-------|----------------------|
| 1 | 0.47 | 0.041 | 0.52 | 0.043 |
| 2 | 0.64 | 0.045 | 0.66 | 0.046 |
| 3 | 0.55 | 0.089 | 0.58 | 0.091 |
| 4 | 0.54 | 0.047 | 0.56 | 0.048 |
| 5 | 0.39 | 0.047 | 0.40 | 0.050 |
| 6 | 0.41 | 0.046 | 0.42 | 0.048 |
| 7 | 0.38 | 0.040 | 0.39 | 0.041 |
| 8 | 0.36 | 0.030 | 0.38 | 0.032 |

main frequency range related to wall deformation, and duration of the ground motion. The k_{hk} concept was found to accurately and consistently predict the deformation of quay walls under various conditions, compared to the simplified dynamic analysis methods. However, the k_{hk} concept is relatively conservative when low-frequency

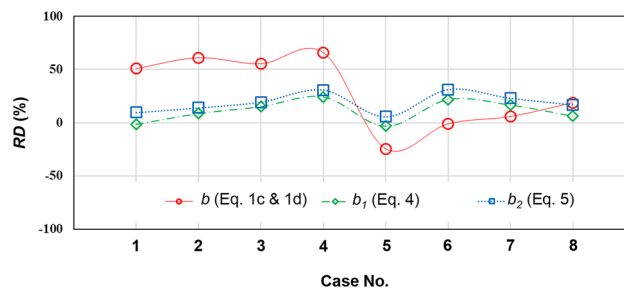


Fig. 11 Relative difference in percentage between the D_h values calculated with the different b values (Eqs. 1c, 1d, 4, and 5) and the measured D_h values for all cases

components are dominant. Thus, the b filter was revised in relation to the low-frequency band. Multiple linear regression analysis was used to derive two revised equations for b , where the independent variables were the wall height and the natural periods of the subsoil and backfill soil or the wall height and natural period of the backfill soil only. The field applicability and reliability of the revised b values were partially verified through evaluations using

the dynamic centrifuge test results and actual records of earthquake-damaged quay walls. The results of this study demonstrated how the k_{hk} concept can be improved and various methods of verifying the performance-based design of gravity-type quay walls. In the future, more accurate regression equations for verifying the performance of a quay wall should be derived by considering a few additional aspects.

First, the actual deformation of quay walls during an earthquake is a combined result of the shear deformation of the subsoil and the relative displacements between the subsoil and the quay wall. However, as the subsoil stiffness of the dynamic centrifuge tests and field records analyzed in this study were mostly high, the applicability of the equations with the revised value of b may be limited for liquefied or loose ground conditions. Therefore, for more comprehensive analyses of the deformation of quay walls, the effect of subsoil shear deformation should be investigated by considering additional experimental variables such as the shape, thickness, material properties, and relative density of the subsoil.

Second, it is necessary to derive appropriate independent variables for the regression analyses by conducting studies on additional influence factors that can affect the main frequency range related to wall deformation, in addition to existing variables constituting the b filter.

Lastly, the reliable databases from physical tests, numerical analyses, and field data for various variables such as the design seismic coefficient of the wall, ground stiffness, and input earthquakes should be constructed to improve the reliability of the regression analysis.

Acknowledgement This research was part of a project titled “Development of performance-based seismic design technologies for advancement in design codes for port structures” funded by the Ministry of Oceans and Fisheries, Korea. This study was also supported by the Basic Research Project of Korea Institute of Geoscience and Mineral Resources (KIGAM).

References

- Al-Atik L, Sitar N (2010) Seismic earth pressures on cantilever retaining structures. *J Geotech Geoenviron Eng* 136(10):1324–1333
- Al-Homoud AS, Tahtamoni W (2000) Comparison between predictions using different simplified Newmarks’ block-on-plane models and field values of earthquake induced displacements. *Soil Dyn Earthq Eng* 19(2):73–90
- Ambraseys NN (1972) Behaviour of foundation materials during strong earthquakes. In: Proceedings of the Fourth European Symposium on Earthquake Engineering, Vol 7, Bulgarian Academy of Sciences, Sofia, pp 11–12
- Anderson DG, Martin GR, Lam I, Wang JN (2008) NCHRP611: Seismic analysis and design of retaining walls, buried structures, slopes and embankments. Transportation Research Board, Washington DC
- Arias A (1970) A measure of earthquake intensity. In: Hansen RJ (ed) Seismic design for nuclear power plants. Massachusetts Institute of Technology Press, Cambridge, pp 438–483
- Bilotta E, Lanzano G, Madabhushi SG, Silvestri F (2014) A numerical round robin on tunnels under seismic actions. *Acta Geotech* 9(4):563–579
- Bozbey I, Gundogdu O (2011) A methodology to select seismic coefficients based on upper bound “Newmark” displacements using earthquake records from Turkey. *Soil Dyn Earthq Eng* 31(3):440–451
- Brandenberg SJ, Mylonakis G, Stewart JP (2015) Kinematic framework for evaluating seismic earth pressures on retaining walls. *J Geotech Geoenviron Eng* 141(7):04015031
- Cai Z, Bathurst RJ (1996) Deterministic sliding block methods for estimating seismic displacements of earth structures. *Soil Dyn Earthq Eng* 15(4):255–268
- Cakir T (2013) Evaluation of the effect of earthquake frequency content on seismic behavior of cantilever retaining wall including soil–structure interaction. *Soil Dyn Earthq Eng* 45:96–111
- Chaudhary B, Hazarika H, Murakami A, Fujisawa K (2018) Countermeasures for enhancing the stability of composite breakwater under earthquake and subsequent tsunami. *Acta Geotech* 13(4):997–1017
- Deyanova M, Lai CG, Martinelli M (2016) Displacement–based parametric study on the seismic response of gravity earth-retaining walls. *Soil Dyn Earthq Eng* 80:210–224
- Dobry R, Idriss IM, Ng E (1978) Duration characteristics of horizontal components of strong-motion earthquake records. *Bull Seismol Soc Am* 68(5):1487–1520
- EN 1998-5 (2004) Eurocode 8: Design of structures for earthquake resistance: Part 5: Foundations, retaining structures and geotechnical aspects. Comité Européen de Normalisation (CEN), Brussels
- Fukunaga Y, Takenobu M, Miyata M, Nozu A, Kohama E (2016) Validation of present seismic design method for gravity-type and sheet pile quay walls by past earthquake-induced damage data of port facilities and reproduced seismic ground motions. National Institute for Land and Infrastructure Management, Ministry of Land, Infrastructure and Transport, Tokyo (in Japanese)
- Garini E, Gazetas G, Anastasopoulos I (2011) Asymmetric ‘Newmark’ sliding caused by motions containing severe ‘directivity’ and ‘fling’ pulses. *Géotechnique* 61(9):733–756
- Ghalandarzadeh A, Orita T, Towhata I, Yun F (1998) Shaking table tests on seismic deformation of gravity quay walls. *Soils Found* 38:115–132
- Hatami K, Bathurst RJ (2000) Effect of structural design on fundamental frequency of reinforced-soil retaining walls. *Soil Dyn Earthq Eng* 19:137–157
- Iai S, Sugano T (2000) Shake table testing on seismic performance of gravity quay walls. In: Proceedings of the 12th World Conference on Earthquake Engineering, New Zealand Society for Earthquake Engineering, Silverstream, pp 1–8
- Ichii K, Iai S, Sato Y, Liu H (2002) Seismic performance evaluation charts for gravity type quay walls. *J Struc Mech Earthq Eng* 19(1):21–31
- Inagaki H, Iai S, Sugano T, Yamazaki H, Inatomi T (1996) Performance of caisson type quay walls at Kobe Port. *Soils Found* 36:119–136
- International Navigation Association (INA) (2001) Seismic design guidelines for port structures. A A Balkema Publishers, London
- ISO 23469:2005 (2005) Bases for design of structures—Seismic actions for designing geotechnical works. International Organization for Standardization (ISO), Geneva
- Jibson RW (2007) Regression models for estimating coseismic landslide displacement. *Eng Geol* 91(2–4):209–218

25. Kang S, Kim B, Bae S, Lee H, Kim M (2019) Earthquake-induced ground deformations in the low-seismicity region: a case of the 2017 M5.4 Pohang, South Korea, earthquake. *Earthq Spectra* 35(3):1235–1260
26. Kim DS, Kim NR, Choo YW, Cho GC (2013) A newly developed state-of-the-art geotechnical centrifuge in Korea. *KSCE J Civ Eng* 17(1):77–84
27. Kim DS, Lee SH, Choo YW, Perdrat J (2013) Self-balanced earthquake simulator on centrifuge and dynamic performance verification. *KSCE J Civ Eng* 17(4):651–661
28. Kim SR, Jang IS, Chung CK, Kim MM (2005) Evaluation of seismic displacements of quay walls. *Soil Dyn Earthq Eng* 25(6):451–459
29. Kinoshita S (1998) Kyoshin net (K-net). *Seismol Res Lett* 69(4):309–332
30. Kramer SL (1996) *Geotechnical earthquake engineering*. Prentice-Hall, New Jersey
31. Lee CJ (2005) Centrifuge modeling of the behavior of caisson-type quay walls during earthquakes. *Soil Dyn Earthq Eng* 25:117–131
32. Lee MG, Ha JG, Manandhar S, Park HJ, Kim DS (2019) Evaluation of performance-based seismic coefficient for gravity-type quay wall via centrifuge tests. *Soil Dyn Earthq Eng* 123:292–303
33. Lee MG, Jo SB, Ha JG, Park HJ, Kim DS (2017) Assessment of horizontal seismic coefficient for gravity quay walls by centrifuge tests. *Géotech Lett* 7(2):211–217
34. Lee SH, Choo YW, Kim DS (2013) Performance of an equivalent shear beam (ESB) model container for dynamic geotechnical centrifuge tests. *Soil Dyn Earthq Eng* 44:102–114
35. Madabhushi GS, Boksmati JI, Torres SG (2019) Modelling the behaviour of large gravity wharf structure under the effects of earthquake-induced liquefaction. *Coast Eng* 147:107–114
36. Meehan CL, Vahedifard F (2013) Evaluation of simplified methods for predicting earthquake-induced slope displacements in earth dams and embankments. *Eng Geol* 152(1):180–193
37. Ministry of Land, Infrastructure and Transport (MLIT) (1999) *Technical standards and commentaries for port and harbour facilities in Japan*. Japan Port and Harbour Association, Tokyo (in Japanese)
38. Ministry of Land, Infrastructure and Transport (MLIT) (2007) *Technical standards and commentaries for port and harbour facilities in Japan*. Japan Port and Harbour Association, Tokyo (in Japanese)
39. Ministry of Land, Infrastructure and Transport (MOLIT) (2012) *Seismic performance evaluation and improvement revision of existing structures (harbours)*. Korea Infrastructure Safety and Technology Corporation, Incheon (in Korean)
40. Ministry of Oceans and Fisheries (MOF) (2014) *Ports and fishing harbours design code*. Ministry of Oceans and Fisheries, Sejong (in Korean)
41. Ministry of Oceans and Fisheries (MOF) (2018) *Comprehensive report for Pohang Port earthquake damage investigation and restoration manual*. Korea Port Engineering Corporation, Seoul (in Korean)
42. Mononobe N, Matsuo H (1929) On the determination of earth pressure during earthquake. In: *Proceedings of World Engineering Congress, Vol 9, World Engineering Congress, Tokyo*, pp 177–185
43. Motamed R, Towhata I (2010) Shaking table model tests on pile groups behind quay walls subjected to lateral spreading. *J Geotech Geoenviron Eng* 136(3):477–489
44. Nagao T, Iwata N (2007) Seismic coefficients of caisson type and sheet pile type quay walls against the level-one earthquake ground motion. *J Struct Eng A* 53A:339–350
45. Nakamura S (2006) Reexamination of Mononobe-Okabe theory of gravity retaining walls using centrifuge model tests. *Soils Found* 46(2):135–146
46. Newland DE, Butler GD (2000) Application of time-frequency analysis to transient data from centrifuge earthquake testing. *Shock Vib* 7(4):195–202
47. Newmark NM (1965) Effects of earthquakes on dams and embankments. *Géotechnique* 15(2):139–160
48. Nishimura S, Takahashi H, Morikawa Y (2012) Observations of dynamic and non-dynamic interactions between a quay wall and partially stabilised backfill. *Soils Found* 52(1):81–98
49. Nozu A, Ichii K, Sugano T (2004) Seismic design of port structures. *J Jpn Assoc Earthq Eng* 4:195–208
50. Okabe S (1924) General theory on earth pressure and seismic stability of retaining wall and dam. *J Jpn Soc Civ Eng* 10:1277–1323
51. Pelekis I, Madabhushi GS, DeJong MJ (2019) Soil behaviour beneath buildings with structural and foundation rocking. *Soil Dyn Earthq Eng* 123:48–63
52. Rathje EM, Abrahamson NA, Bray JBD (1998) Simplified frequency content estimates of earthquake ground motions. *J Geotech Geoenviron Eng* 124(2):150–159
53. Richards R Jr, Elms DG (1979) Seismic behavior of gravity retaining walls. *J Geotech Geoenviron Eng* 105:449–464
54. Santhoshkumar G, Ghosh P (2020) Seismic stability analysis of a hunchbacked retaining wall under passive state using method of stress characteristics. *Acta Geotech* 15(10):2969–2982
55. Schofield AN (1980) *Cambridge geotechnical centrifuge operations*. *Géotechnique* 30(3):227–268
56. Tso WK, Zhu TJ, Heidebrecht AC (1992) Engineering implication of ground motion A/V ratio. *Soil Dyn Earthq Eng* 11(3):133–144
57. Veletsos AS, Younan AH (1997) Dynamic response of cantilever retaining walls. *J Geotech Geoenviron Eng* 123(2):161–172
58. Wagner N, Sitar N (2016) On seismic response of stiff and flexible retaining structures. *Soil Dyn Earthq Eng* 91:284–293
59. Wei YC, Lee CJ, Hung WY, Chen HT (2010) Application of Hilbert-Huang transform to characterize soil liquefaction and quay wall seismic responses modeled in centrifuge shaking-table tests. *Soil Dyn Earthq Eng* 30(7):614–629
60. Werner SD (1998) *Seismic guidelines for ports*. Technical Council on Lifeline Earthquake Engineering (TCLEE). ASCE, New York
61. Whitman RV, Liao S (1985) *Seismic design of gravity retaining walls*. Miscellaneous Paper GL-85-1. US Army Engineer Waterway Experiment Station, Vicksburg, MS
62. Zarrabi-Kashani K (1979) *Sliding of gravity retaining wall during earthquakes considering vertical acceleration and changing inclination of failure surface*. Dissertation, Massachusetts Institute of Technology
63. Zeng X (1998) Seismic response of gravity quay walls. I: Centrifuge modeling. *J Geotech Geoenviron Eng* 124(5):406–417

Publisher's Note Springer Nature remains neutral with regard to jurisdictional claims in published maps and institutional affiliations.